Teleseismic scattered-wave imaging of Japan Subduction zones

YoungHee Kim[1]
Hitoshi Kawakatsu[2]

[1] School of Earth and Environmental Sciences, Seoul National University
younghkim@snu.ac.kr
[2] Earthquake Research Institute, University of Tokyo, Japan
hitosi@eri.u-tokyo.ac.jp

Abstract

The Japan arcs exhibit significant along-arc transition in slab geometry, subduction-driven magmatic activity, and plate coupling state. We exploit teleseismic data from dense Hi-net array to define the present-day subduction-zone geometry and to constrain the plate boundary dynamics in response to variable slab geometries and physical properties of the subducting material. We retrieve backscattered (or reverberated) body-wave phases in addition to direct Ps (incident P wave forward-scattered as an S wave) and apply the teleseismic migration method based on the Generalized Radon Transform (Bostock et al., 2001) to accurately define both Pacific and Philippine Sea plate subduction structures. This method inverts the scattered waves for sharp variations in the Earth's elastic properties beneath the high-density array using analytical expressions for their travel-times and amplitudes (Bostock et al., 2001). The four scattering modes (Ps, PpPs, PpSs|v, and PpSs|h) are sensitive to S-wave velocity perturbations (dVs/Vs) and are combined to form a single composite image. As more migrated phases are stacked in, the artifacts due to cross-mode contamination (i.e., parallel echoes of the real structure) become attenuated while energy mapped to its correct depth is sharply imaged. Preliminary images show complex slab structures down to a depth of 200 – 300 km with significant along-arc velocity variations at the top of the plate. Such differences in the velocity structures may indicate different hydration state due to slab age and/or presence of low-strength materials.

Key words: seismic imaging, teleseismic migration, scattered wavefield, seismicity, subduction zone process, Japan subduction zone

1. Introduction

The Japan subduction zone shows variable progression of slab-dip angles along the trench. The Pacific and Philippine Sea oceanic plates are subducting beneath the Japan arcs, and in particular, complex plate geometry is expected at the region where the two plates meet at the eastern and northern parts of Central and SW Japan. In addition to significant along-strike slab-dip variations, seismological and geochemical properties in NE and SW Japan arc systems are dominantly controlled by convergence rates, thermal structure, and subduction input and melting.

Dense seismic dataset from Hi-net array (Figure 1) reveal several important constraints that have enlightened interesting and unusual subduction dynamics in Japan subduction zone (Matsubara et al., 2008, and references therein). In this paper, we provide high-resolution images based on the migration of scattered teleseismic body waves (Bostock et al., 2001, and references therein), with local earthquakes to improve the estimation of the subduction structure of Pacific and Philippine Sea plates. Our images will provide insight into the process of subducting young and old oceanic lithospheres and upper-plate deformation in response to the subduction. Also, the images will clarify the relationship between seismicity and imaged slabs.

2. Data analysis and teleseismic imaging

In order to accurately define the subduction zone structure, we use two-dimensional generalized radon transform-based migration (hereafter 2-D GRT) method. First, we use the 2-D GRT method to identify the location and magnitude of the discontinuities separating regions of differing seismic impedance. This method inverts scattered waves within the teleseismic P-wave coda for sharp variations in the Earth's elastic properties beneath high-density arrays (Bostock and Rondenay, 1999; Bostock et al., 2001; Rondenay et al., 2005; Rondenay, 2009). The method has been extensively applied to array datasets in various subduction zones to constrain seismic properties of the subduction system and also to infer the subduction dynamics (e.g., Alaska (Rondenay et al., 2008, 2010; Kim et al., 2014),

Cascadia (Bostock et al., 2002; Abers et al., 2009), Costa Rica and Nicaragua (MacKenzie et al., 2010), western Hellenic (Suckale et al., 2009; Pearce et al., 2012), Mexico (Kim et al., 2012, 2013, 2014), and Peru (Kim et al., 2015). Kim et al. (2012) described the imaging procedure in detail.

We retrieve high-quality teleseismic P waves recorded from the Hi-net array for earthquakes in 2006 (Figure 2a). We follow the data selection and preprocessing procedures described in Pearce et al. (2012) and Kim et al. (2012). In the migration images, inversions determine the velocity perturbations with respect to the background velocity model (Table 1; Ulkawa et al., 1984) needed to produce the scattered wavefield (Rondenay et al., 2001, 2005). Both P- and S-wave velocities are shown with a red to blue color scale, which represents negative (slower) to positive (faster) velocity perturbations (Figures 2b-f and 3). Velocity discontinuities in the migration images are identified by cross-overs in the color scale, with red-to-blue denoting an increase in velocity with depth (e.g. Moho) and blue-to-red denoting a decrease in velocity with depth (Rondenay et al., 2005). We use a frequency filter of 0.03 – 0.2 Hz in the migration as used in imaging of other subduction zones (Kim et al., 2012, and references there in). We also try a filter of 0.03 – 0.3 Hz to suppress noise near the coastal stations and to enhance image coherence.

Each mode contributions to the S-velocity perturbation (dVs/Vs) from forward-scattered (Ps) and backscattered phases (PpPs, PpSs|v, and PpSs|h), along with dVp/Vp from PpPp show the subducting slabs with different magnitudes although each response is not fully always clear (Figures 2b-f). On its own, the Ps modes recover the dipping structures the best because Ps mode is most sensitive to steeply dipping features, however it does not resolve the full thickness of the dipping layer (7 – 10 km) due to the lower frequency filter of 0.03 – 0.2 (or 0.3) Hz used in the migration and the lower volume resolution of the Ps mode (Rondenay et al., 2005). We apply different weights to the four scattering modes (5 for Ps, 3 for PpPs, 0.5 for PpSs|v, and 0.5 for PpSs|h) to reduce the contributions from scattering modes that display weak responses (Rondenay et al., 2001).

For imaging, we set profile azimuths, which are nearly trench perpendicular (Figure 1). We divide the events in four backazimuth groups to examine azimuthal contribution to the migration image. We expect and observe that the event contributions from the south (Figure 1a) are essential to clearly delineate the subducting slabs. The migration is demonstrated as an

effective method if teleseismic earthquakes occurring over a wide (ideally uniform) azimuthal distribution are stacked (Rondenay et al., 2005; Kim et al., 2012). Figure 3 shows composite dVs/Vs images with seismicity for five profiles (P4 – P8 in Figure 1), which clearly show the subducting Pacific slab.

3. Slab geometries and seismicity

The distribution of regional earthquakes has provided the most robust way to characterize the geometry of the subducted slabs although the seismicity on its own cannot accurately provide the oceanic crust-mantle and/or continental crust-mantle interfaces with high precision. Regional tomographic images (e.g., Matsubara et al., 2008, and references therein) can also reveal the presence of the subducting slabs shown as a fast velocity anomaly beneath the seismic array. However, the estimates of their along-strike dips as well as geometries, and velocity variations within the oceanic crust (i.e., termination depth of dehydration reaction in the oceanic crust) cannot be accurately constrained due to the depth limitation of regional dataset. The location and geometry of sharp subduction interfaces (assuming substantial velocity contrast across the interfaces) can be well resolved by using the converted phases. The receiver function studies by Kawakatsu and Watada (2007) traced a strong negative conversion at the top of the subducting oceanic crust of the Pacific plate beneath NE Japan down to ~100 km depth.

Detailed mapping of inverted seismic parameters revealed that the upper part of the subducting oceanic crust is highly heterogeneous, and is composed of mechanically weak hydrous minerals (Kim et al., 2010, 2013, 2015). The presence of such hydrous minerals and/or high pore fluid pressure in forearc system reduce the seismic velocity to considerably less than the velocity of the surrounding mantle (Audet et al., 2009; Kim et al., 2010; Audet and Kim, 2016). Observed low velocities and higher Vp/Vs (and Poisson's ratio) at the dipping oceanic crust before the termination depth imply an active dewatering process in the subduction system. In NE Japan, the hydrous minerals become unstable at pressure and temperature conditions at 80 – 100 km and are dehydrated to become anhydrous eclogitic oceanic crust (Kawakatsu and Watada, 2007).

Figure 3 shows a dipping Pacific slab in NE Japan. We observe that the slab is dipping in ~30 degrees in five different regions, and the dipping angle slightly decreases towards SW (Figure

3). The largest Vs reduction is observed in the dipping oceanic crust from the coast (horizontal distance = 0 km) to inland region (horizontal distance < ~100 km) (Figure 3). The low-velocity termination depth cannot be fully constrained at the moment from the images (Figure 3). More earthquakes are needed to be incorporated to enhance the quality of the image for the dipping slab as well as upper-plate Moho. The location for the upper-plate Moho can be traced from Figures 3a, c, d, and e.

References

Abers, G. A., L. S. MacKenzie, S. Rondenay, Z. Zhang, A. G. Wech, and K. C. Creager (2009), Imaging the source region of Cascadia tremor and intermediate-depth earthquakes, Geology, 37(12), 1119–1122, doi:10.1130/G30143A.1.

Audet, P., M. G. Bostock, N. I. Christensen, and S. M. Peacock (2009), Seismic evidence for overpressured subducted oceanic crust and megathrust fault sealing, Nature, 457, 76–78, doi:10.1038/nature07650.

Audet, P., and Y. Kim (2016), Teleseismic constraints on the geological environment of episodic slow earthquake in subduction zone forearcs: A review, Tectonophysics (Invited Review Articles), 670, 1-15, doi:10.1016/j.tecto.2016.01.005.

Bostock, M. G., and S. Rondenay (1999), Migration of scattered teleseismic body waves, Geophys. J. Int., 137, 732–746, doi:10.1046/j.1365-246x.1999.00813.x.

Bostock, M. G., S. Rondenay, and J. Sharagge (2001), Multiparameter two-dimensional inversion of scattered teleseismic body waves: 1. Theory for oblique incidence, J. Geophys. Res., 106(B12), 30,771–30,782, doi:10.1029/2001JB000330.

Bostock, M.G., R. D. Hyndman, S. Rondenay, and S. M. Peacosk (2002), An inverted continental Moho and the serpentinization of the forearc mantle, Nature, 417, 536–538.

Kawakatsu, H., and S. Watada (2007), Seismic evidence for deep‐water transportation in the mantle, Science, 316, 1468‐1471, doi:10.1126/ science.1140855.

Kim, Y., R.W. Clayton, and J. M. Jackson (2010), The geometry and seismic properties of the subducting Cocos plate in central Mexico, J. Geophys. Res., 115, B06310, doi:10.1029/2009JB006942.

Kim, Y., R. W. Clayton, and F. Keppie (2011), Evidence of a collision between the Yucatán Block and Mexico in the Miocene, Geophys. J. Int., 187, 989–1000, doi:10.1111/j.1365246X.2011.05191.x.

Kim, Y., M. S. Miller, F. D. Pearce, and R. W. Clayton (2012), Seismic imaging of the Cocos plate subduction zone system in central Mexico, Geochem. Geophys. Geosyst., 13, Q07001, doi:10.1029/2012GC004033.

Kim, Y., R. W. Clayton, P. D. Asimow, and J. M. Jackson (2013), Generation of talc in the mantle wedge and its role in subduction dynamics in central Mexico, Earth and Planetary Science Letters, 384, 81–87, doi:10.1016/j.epsl.2013.10.006.

Kim, Y., G. A. Abers, J. Li, D. Christensen, J. Calkins, and S. Rondenay (2014), Alaska Megathrust 2: Imaging the megathrust zone and Yakutat/Pacific plate interface in the Alaska subduction zone, J. Geophys. Res., 119, doi:10.1002/2013JB010581.

Kim, Y., and R. W. Clayton (2015), Seismic properties of the Nazca oceanic crust in southern Peruvian subduction system, Earth and Planetary Science Letters, 429, 110–121, http://dx.doi.org/10.1016/j.epsl.2015.07.055.

MacKenzie, L. S., G. A. Abers, S. Rondenay, and K. M. Fischer (2010), Imaging a steeply dipping subducting slab in Southern Central America, Earth Planet. Sci. Lett., 296, 459–468, doi:10.1016/j.epsl.2010.05.033.

Matsubara, M., K. Obara, and K. Kasahara (2008), Three-dimensional P- and S-wave velocity structures beneath the Japan Islands obtained by high-density seismic stations by seismic tomography, Tectonophysics, 454, 86–103.

Pearce, F. D., S. Rondenay, M. Sachpazi, M. Charalampakis, and L. H. Royden (2012), Seismic investigation of the transition from continental to oceanic subduction along the western Hellenic Subduction Zone, J. Geophys. Res., doi:10.1029/ 2011JB009023.

Rondenay, S., M. G. Bostock, and K. M. Fischer (2005), Multichannel inversion of scattered teleseismic body waves: Practical considerations and applicability, in Seismic Earth: Array Analysis of Broadband Seismograms, Geophys. Monogr. Ser., vol. 157, edited by A. Levander and G. Nolet, pp. 187–203, AGU, Washington, D. C., doi:10.1029/157GM12.

Rondenay, S., G. A. Abers, and P. E. van Keken (2008), Seismic imaging of subduction zone metamorphism, Geology, 36, 275–278.

Rondenay, S. (2009), Upper mantle imaging with array recordings of converted and scattered teleseismic waves, Surv. Geophys., 30, 377–405, doi:10.1007/s10712-009-9071-5.

Rondenay, S., L. G. J. Montesi, and G. A. Abers (2010), New geophysical insight into the origin of the Denali volcanic gap, Geophys. J. Int., 182, 613–630, doi: 10.1111/j.1365-246X.2010.04659.x.

Suckale, J., S. Rondenay, M. Sachpazi, M. Charalampakis, A. Hosa, and L. H. Royden (2009), High-resolution seismic imaging of the western Hellenic subduction zone using teleseismic scattered waves, Geophys. J. Int., 178(2), 775–791, doi:10.1111/j.1365-246X.2009.04170.x.

Ukawa, M., M. Ishida, S. Matsumura, and K. Kasahara (1984), Hypocenter determination method of the Kanto-Tokai observational network for microearthquakes, Res. Notes Nat. Res. Centre Disaster Prevention, 53, 1–88.

Table 1. One-dimensional reference model for migration (Ulkawa et al., 1984)

Layer	Depth ranges (km)	Vp (km/s)	Vs (km/s)	Density (g/cm^3)
1	0 – 10	5.5	3.25	2.53
2	10 – 20	5.98	3.49	2.68
3	20 – 32	6.51	3.74	2.85
4	32 – 50	7.2	4.07	3.07
5	50 – 100	7.85	4.43	3.28
6	100 – 150	8.0	4.5	3.33
7	150 – 200	8.12	4.53	3.37
8	200 – 250	8.26	4.6	3.41
9	250 – 300	8.42	4.68	3.46
10	300 – 350	8.58	4.76	3.52
11	350 – 400	8.75	4.85	3.57

Figure List

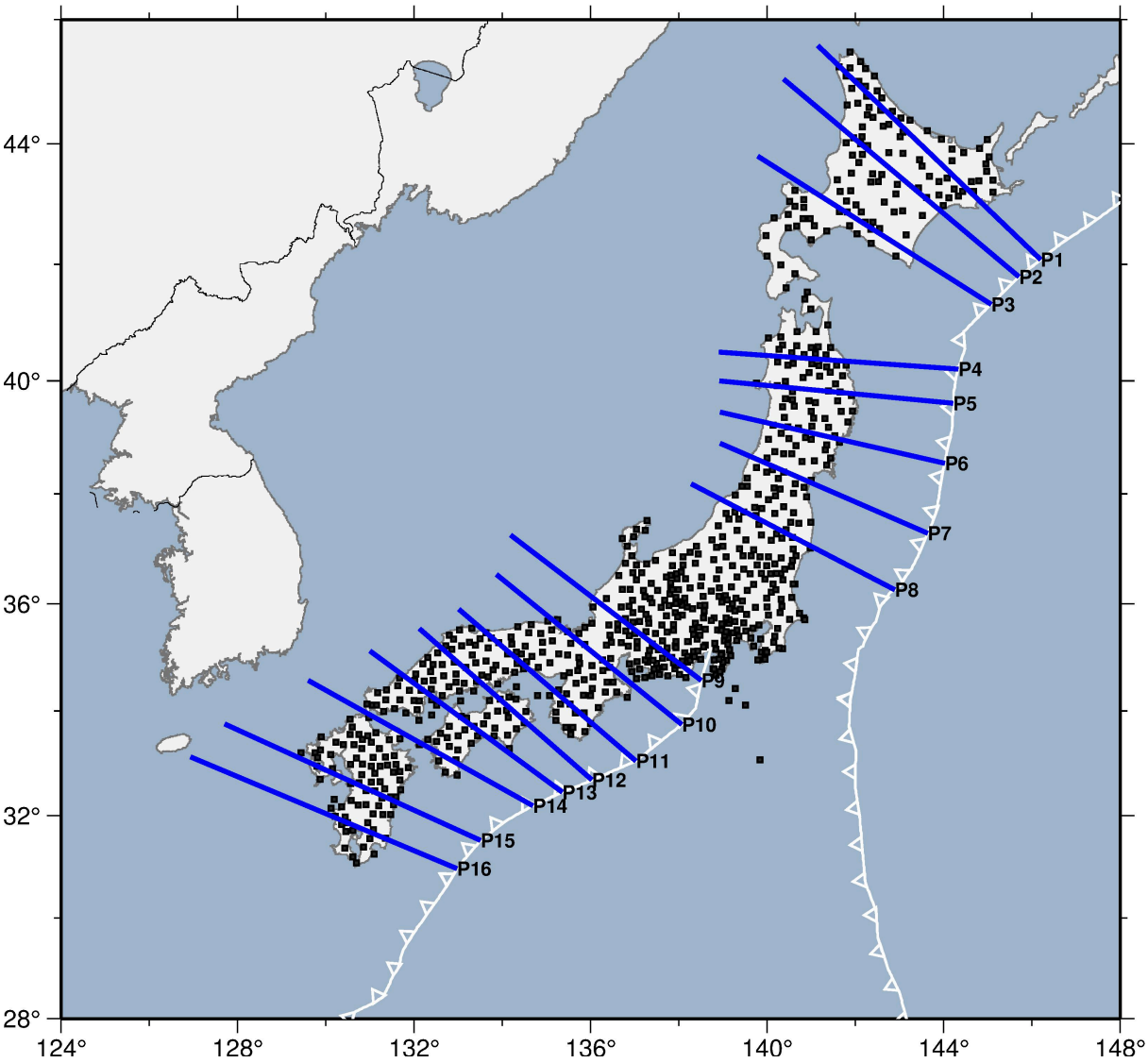

Figure 1. Map showing Hi-net stations (black square) and 16 profiles (denoted as P1 – P16; blue line) for teleseismic migration. Trench location is marked as white line. Note that in this report, we only show images along the profiles P4 – P8, which sample NE Japan (see Figures 2 and 3).

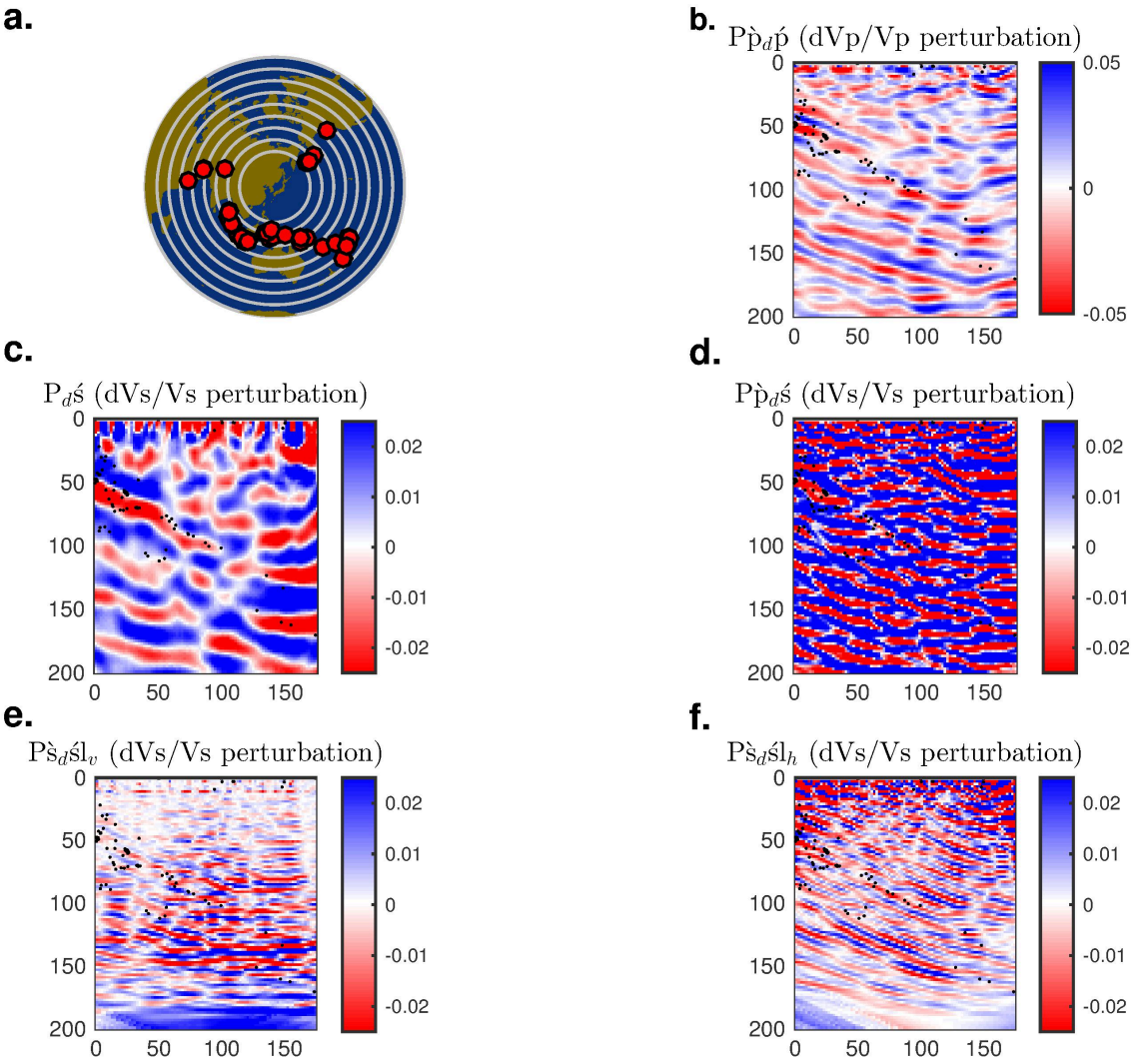

Figure 2. Images showing individual mode contributions. (a) Teleseismic earthquake locations (shown as red dots) used in the analysis. (b–f) Contributions from each scattering modes for one forward mode (Pds) and four backscattered modes (Ppdp, Ppds, Psds|v, and Psds|h), showing the 175 km transect (profile P5 in Figure 1) across NE Japan. 0 km in the horizontal axis marks the location of the coast towards the Pacific ocean. Red to blue color scale represents negative (slower) to positive (faster) P- and S-wave velocity perturbations relative to regional velocity model (Table 1). Each panel in b-f includes seismicity as black dots. Note that this profile P5 is the same profile that Kawakatsu and Watada (2007) used for their receiver function imaging.

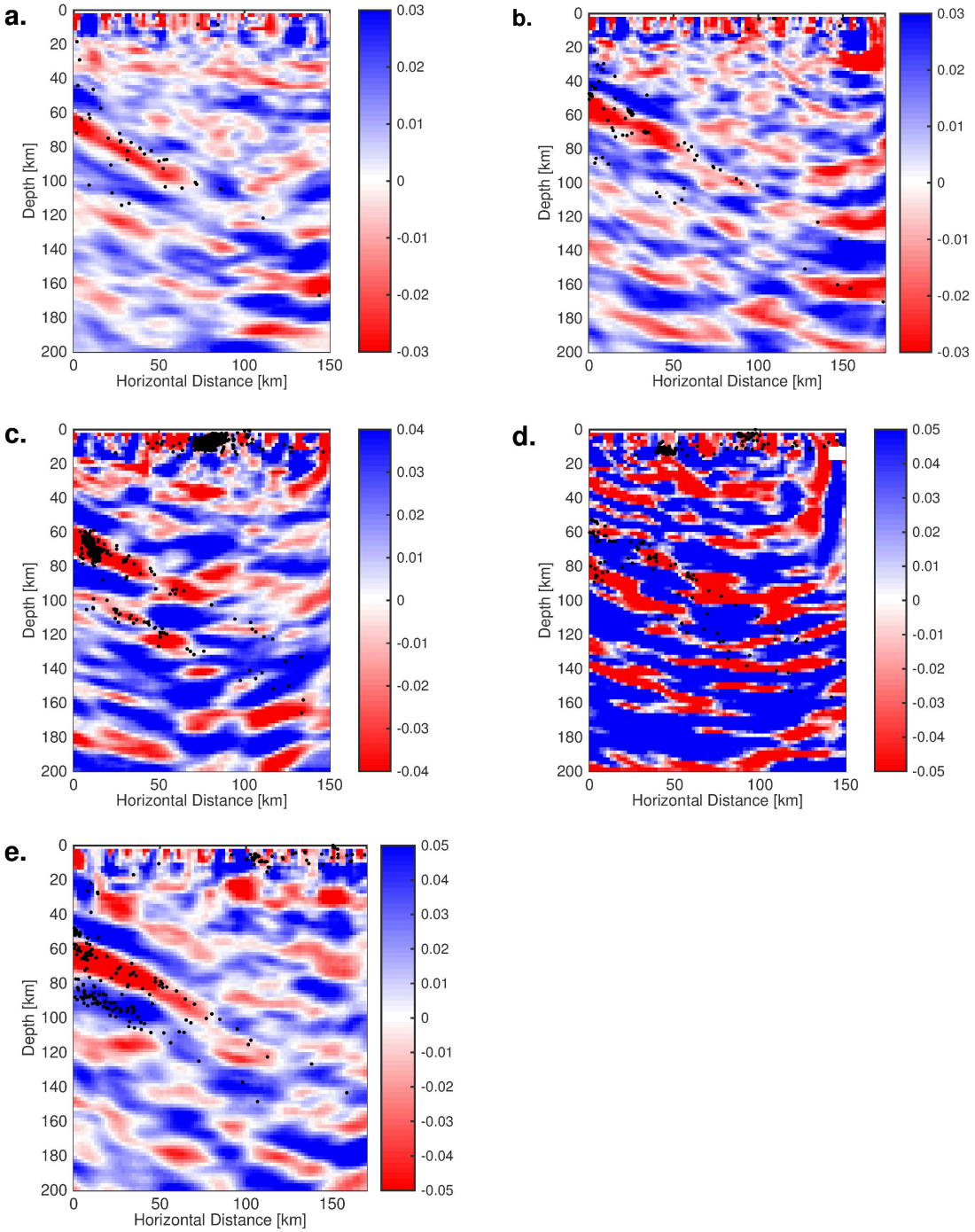

Figure 3. Composite dVs/Vs images for five profiles (P4 – P8 in Figure 1 for panels a – e). Individual mode shown in Figure 2 are stacked together to form the images with the weight, w1 = 5 for Pds, w2 = 3 for Ppds, w3 = 0.5 for Psds|v and w4 = 0.5 for Psds|h, based on the rationale developed in Rondenay et al. (2001). Note that 0 km in the horizontal axis marks the location of the coast towards the Pacific ocean.